DEPARTMENT OF PHYSICS

ATMOSPHERIC, OCEANIC AND PLANETARY PHYSICS

SO_2 volcanic plume retrieval using TES nadir measurements.

Part I: Information content, singular vector decomposition analysis and microwindows computation.

S. Corradini[1], C. Piccolo, C. D. Rodgers, A. Dudhia, R. G. Grainger
Atmospheric, Oceanic and Planetary Physics, Clarendon Laboratory, University of Oxford, U.K.

AOPP Memorandum 2005.1

August 2005

University of Oxford

[1]on leave from *Materials and Environment Engineering Department, University of Modena and Reggio Emilia*, Italy

Abstract

This work investigates the feasibility of using the nadir Tropospheric Emission Spectrometer (TES) measurements to retrieve the abundance and altitude dependence of sulphur dioxide from a volcanic plume.

TES, one of the four instruments on board on NASA's Aura satellite, is a high-resolution, infrared (650 - 2250 cm^{-1}) imaging Fourier transform spectrometer that observes both in the nadir and in the limb with a high spectral resolution (from 0.1 to 0.025 cm^{-1}).

This study has been carried out using an information content approach which describes how many independent pieces of information can be extract from the measurements. It has been applied for different plume configurations and SO_2 column abundances.

The extremely low information content obtained suggests the use of a singular vector decomposition (SVD) approach to reduce the instrumental noise. The SVD reconstructed spectra with reduced noise increases the information content. As an example a tropospheric plume of 150 DU has only 0.1 degrees of freedom for signal (DFS) but this improve to 3 DFS using an SVD approach.

A procedure to optimise the selection of the spectral measurements is also described.

Contents

1 Introduction

During eruptions volcanoes emit large quantity of gases and particles that have important effects on the atmosphere and climate. The most abundant gases typically released into the atmosphere from volcanic systems are water vapour (H_2O), carbon dioxide (CO_2) and sulphur dioxide (SO_2). Volcanoes also release smaller amounts of other gases as hydrogen sulphide (H_2S), hydrogen (H_2), helium (He), carbon monoxide (CO), hydrogen chlorine (HCl), hydrogen fluorine (HF), nitrogen (N) and argon (Ar). In addition to the release of a number of gases, an explosive eruption also ejects solid rock fragments and ash into the air. The largest fragments fall back to the round near the vent while the ash continues rising forming an eruption column which then follows the local wind patterns (Grainger and Highwood, 2003). Ash size distributions are approximately multimode log-normal distributions with a nucleation mode ($r_{\mathrm{mode}} < 0.05\,\mu$m), an accumulation mode ($r_{\mathrm{mode}} \sim 0.05$–$0.5\,\mu$m), and one or more giant modes ($r_{\mathrm{mode}} > 0.5\,\mu$m). The nucleation mode is composed of sulphuric acid-water drops (Hobbs et al., 1991), where the H_2SO_4 is produced either in the volcanic throat or by gas to particle conversion of the SO_2 in the volcanic plume. The accumulation and giant modes are thought to be composed of silicate particles.

Strong perturbations to atmospheric chemistry and radiation are caused by the volcanically enhanced stratospheric aerosol layer composed of H_2SO_4 particles. Such sulphate aerosol mainly scatter solar radiation back to the space, with the immediate effect of reducing the solar irradiance at the ground and causing a negative radiative forcing (Grainger and Highwood, 2003). Additionally the aerosol also absorbs long-wave radiation from the surface and lower atmosphere that would otherwise be emitted to space (Grainger et al., 1993). Some of this radiation is re-emitted back towards the Earth's surface. This results in a small positive radiative forcing. Generally, however, this effect is overwhelmed by the negative radiative forcing (Stenchikov et al., 1998). The radiative effects caused by larger and heavier particles ejected by the eruption, as dust and ash, tend to have an impact on the radiation budget on smaller spatial and temporal scales because they quickly precipitate from the atmosphere.

Eruptions that do not penetrate into the stratosphere are usually regarded as being unimportant for long-term or local climate impacts. However, if such an effusive eruption persists with any strength for an extended period of time, it can at least produce a large radiative forcing over local or regional scales. Such tropospheric eruptions can produce local damage to population, cattle, crops and environment and can be also extremely hazardous to aircrafts (Casadevall et al., 1994). The study of the volcanic gaseous emission provides important insights into subsurface magmatic processes (Gerlach et al., 1985; Casadevall et al.,1987), and emitted gas composition and flux variations can help to predict eruptive activity (Malinconico et al., 1979; Malinconico et al., 1987; Caltabiano et al., 1994).

Remote sensing is one of the most suitable techniques to detect volcanic emissions due to the sporadic nature of volcanic eruptions and the large geographic extent of volcanoes. The first satellite data used for SO_2 stratospheric volcanic eruption retrieval were the Total Ozone Mapping Spectrometer (TOMS) ultraviolet measurements (Krueger et al., 1983; Krueger et al., 1990). In 1993 Read *et al*. used the microwave measurements of the Microwave Limb Sounder (MLS), on board on NASA's Upper Atmosphere Research Satellite (UARS), for the Mt. Pinatubo volcano eruption SO_2 retrieval. More recently the Moderate Resolution Imaging Spectrometer (MODIS) was used to estimate the SO_2 of some eruptions (Watson et al., 2004) and the Thermal Infrared (TIR) bands of the Advanced Spaceborne Thermal Emission and Reflection Radiometer (ASTER) were used to compute SO_2 map

of a volcanic plume in the low troposphere (Urai et al., 2004). SO_2 volcanic columnar content have been retrieved using the High Resolution Infrared Spectrometer (HIRS) (Prata et al., 2004) and the Atmospheric Infrared Sounders (AIRS) (Prata et al. submitted).

In this work the Tropospheric Emission Spectrometer (TES) nadir measurements are used to investigate the feasibility of retrieving volcanic plume sulphur dioxide amounts and its altitude.

Section (2) briefly describes the optimal estimation inversion technique, the error sources and information content theory. Section (3) summarises the main characteristics of TES instrument. In Section (4) the information content approach has been applied to two different SO_2 configurations (a plume placed in the troposphere and in stratosphere) and SO_2 columnar abundances. Section (5) describes the singular vector decomposition theory used for the measurements noise reduction and its application to TES measurements. In Section (6) we report the results of the microwindow selection and in Section (7) the conclusion are presented.

2 Background

The optimal estimation (OE) technique provides a natural solution to the ill-conditioning problems typically found in remote sensing atmospheric retrieval applications; it combines information on the state vector contained in the measurement with an a priori information on the state vector itself.

This section is entirely based on the publications of Rodgers (Rodgers, 1990; Rodgers, 2000).

2.1 Optimal Estimation inversion technique

For any remote measurement, the quantity measured, $\mathbf{y}$, is some vector valued function $\mathbf{F}$ of the unknown *state vector* $\mathbf{x}$, and of some other set of parameters $\mathbf{b}$ not included in the *state vector*. Therefore we write the relationship between the *measurements vector* ($\mathbf{y} \in \mathbb{R}^m$) and the *state vector* ($\mathbf{x} \in \mathbb{R}^n$) as:

$$\mathbf{y} = \mathbf{F}(\mathbf{x}, \mathbf{b}) + \epsilon \tag{1}$$

where $\epsilon \in \mathbb{R}^m$ is the *measurements error* vector and $\mathbf{F} : \mathbb{R}^n \rightarrow \mathbb{R}^m$ is the *forward model* (FM) that describes the physics of the measurements and maps state space to measurement space.

In the general atmospheric retrieval case, as in SO_2 retrieval, the problem described by equation (1) is not linear. In addition an analytical solution to express the state vector in terms of the measurement vector does not exist. An approximate solution can be found using a numerical iterative procedure obtained from linearising the forward model about some reference state $\mathbf{x_0}$:

$$\mathbf{y} - \mathbf{F}(\mathbf{x_0}) = \frac{\partial \mathbf{F}(\mathbf{x})}{\partial \mathbf{x}}(\mathbf{x} - \mathbf{x_0}) + \epsilon = \mathbf{K}(\mathbf{x} - \mathbf{x_0}) + \epsilon \tag{2}$$

where $\mathbf{K}$ is the *weighting function* (WF) matrix of dimension $m \times n$ and describe the measurement sensitivity to the state. Each element of $\mathbf{K}$ is the partial derivative of a spectrum with respect to a state vector element:

$$K_{i,j} = \frac{\partial F_i(x)}{\partial x_j}, (\forall i = 1, \ldots, m; \forall j = 1, \ldots, n) \tag{3}$$

For $m > n$ there is not an unique solution that maps the measurements in the state space. We have to use additional constraints to select an acceptable solution, for example using an a priori information.

For moderately nonlinear problems, defined when FM is linear over the domain of the retrieval errors, it can be shown (Rodgers, 2000) that the expected value of *state vector* $\mathbf{x}_{i+1} \in \mathbb{R}^n$ for the $(i+1)^{th}$ iteration is given by:

$$\mathbf{x}_{i+1} = \mathbf{x_a} + \mathbf{S_a}\mathbf{K}_i^T(\mathbf{K}_i\mathbf{S_a}\mathbf{K}_i^T + \mathbf{S}_\epsilon)^{-1}[\mathbf{y} - \mathbf{y}_i + \mathbf{K}_i(\mathbf{x}_i - \mathbf{x_a})] \tag{4}$$

where $\mathbf{K}_i$ is the WF matrix for the i^{th} iteration, $\mathbf{y}_i = \mathbf{F}(\mathbf{x}_i)$, $\mathbf{S}_\epsilon$ is the *measurement covariance* matrix (the diagonal elements are the variances of $\mathbf{y}$ ($\sigma_\epsilon{}^2$)), $\mathbf{x}_a$ is the *a priori state vector* and $\mathbf{S_a}$ is the *a priori covariance* matrix (the diagonal elements are the variances of $\mathbf{x_a}$ ($\sigma_\mathbf{a}{}^2$)). For $i = 0$, $\mathbf{x}_0 \equiv \mathbf{x_a}$. The iterative process ends when given convergence criteria are satisfied.

2.2 Error Analysis

The retrieval error has four components: *retrieval noise, smoothing error, forward model parameter error* and *forward model error*. They will be briefly described as follows.

Retrieval noise

The *retrieval noise* is the error induced by the error in the measurements. Its covariance matrix (*noise covariance matrix* ($\mathbf{S_m}$)) is defined as:

$$\mathbf{S_m} = \mathbf{G}\mathbf{S}_\epsilon\mathbf{G}^T \tag{5}$$

where $\mathbf{G}$ is the *gain matrix* that represents the sensitivity of the retrieval ($\mathbf{R}$) to the measurements ($\mathbf{y}$):

$$\mathbf{G} = \partial\mathbf{R}/\partial\mathbf{y} = (\mathbf{K}^T\mathbf{S}_\epsilon{}^{-1}\mathbf{K} + \mathbf{S_a}{}^{-1})^{-1}\mathbf{K}^T\mathbf{S}_\epsilon{}^{-1} = \mathbf{S_a}\mathbf{K}^T(\mathbf{K}\mathbf{S_a}\mathbf{K}^T + \mathbf{S}_\epsilon)^{-1} \tag{6}$$

Smoothing Error

The *smoothing error* represents the way in which the observing system smooths the profile. The *smoothing error covariance* matrix is defined as:

$$\mathbf{S_s} = (\mathbf{A} - \mathbf{I_n})\mathbf{S_a}(\mathbf{A} - \mathbf{I_n})^T \tag{7}$$

where $\mathbf{I_n}$ is the unit matrix in the state vector space and $\mathbf{A} = \partial\hat{\mathbf{x}}/\partial\mathbf{x} = \mathbf{GK}$ is called the *averaging kernel* matrix. $\mathbf{A}$ represents the sensitivity of the retrieval ($\hat{\mathbf{x}}$) to the true state ($\mathbf{x}$). The $\mathbf{A}$ rows can be regarded as smoothing functions; in an ideal inverse method, $\mathbf{A}$ would be a unit matrix. $\mathbf{A}$ rows are generally peaked functions whose half-width is a measure of the spatial resolution of the observing system.

In the absence of other sources of error the *total retrieval error* ($\hat{\mathbf{S}}$) is defined as the sum between the *noise* and the *smoothing error*:

$$\hat{\mathbf{S}} = \mathbf{S_m} + \mathbf{S_s} \tag{8}$$

Forward Model Parameter Error

The *FM parameter errors* are due to errors in the forward model physical parameters. Assuming that the uncertainties on forward model parameters ($\mathbf{b}$) are characterised by Gaussian statistics with error covariance $\mathbf{S_b}$, the FM parameter *error covariance* matrix ($\mathbf{S}_f$) becomes:

$$\mathbf{S_f} = \mathbf{G}\mathbf{K_b}\mathbf{S_b}\mathbf{K_b}{}^T\mathbf{G}^T \tag{9}$$

These parameters are those quantities that influence the measurements, they are known with some accuracy and are not intended as quantities to be retrieved. In the current retrieval the aim of the FM parameters error calculation is to understand the effect of atmospheric and surface parameter uncertainty on the retrieval.

Forward Model Error

An additional source of error on the retrieved profile arises from approximations made in the FM itself. This error source is treated as systematic because its effect manifests as an offset on the retrieved state:

$$\epsilon_{fm} = \mathbf{G}\Delta\mathbf{F} \tag{10}$$

where $\Delta\mathbf{F} = \mathbf{f}(\mathbf{x},\mathbf{b}) - \mathbf{F}(\mathbf{x},\mathbf{b})$ and $\mathbf{f}(\mathbf{x},\mathbf{b})$ is the *forward function* that describes the complete physics of the measurements.

2.3 Information Content

The information content represents how many independent pieces of information can be extracted from the measurements. The information content allows us to understand if the measurement can improve our knowledge on the retrieved quantities. The information content is described by the *Degrees of Freedom for Signal* (DFS) and the *Shannon information content* (H). DFS can be interpreted as the number of linear combinations of the *state vector* that can be independently retrieved from the measurements. It is given by:

$$\mathrm{DFS} = \sum_{i=1}^{m} \frac{\lambda_i^2}{1+\lambda_i^2} = tr(\mathbf{A}) \tag{11}$$

where λ_i are the singular values of $\tilde{\mathbf{K}} = \mathbf{S}_\epsilon^{-\frac{1}{2}}\mathbf{K}\mathbf{S}_a^{\frac{1}{2}}$ and $tr(\mathbf{A})$ is the trace of $\mathbf{A}$.

If *n* is the dimension of the state vector, DFS$= n$ when the measurements completely determine the state, and DFS$= 0$ when there is no information at all in the measurements.

The *Shannon information content* (H) of a measurement can be defined qualitatively as the scalar quantity which relates prior knowledge to knowledge improved by making the measurements. It is computed as the entropy difference between the final (after the measurements) and the initial system state, and it is given by:

$$H = \frac{1}{2}\sum_{i=1}^{m} \ln(1+\lambda_i^2) = -\frac{1}{2}\ln|\mathbf{I}_n - \mathbf{A}| \tag{12}$$

where $\mathbf{I}_n$ is the n-dimension identity matrix and $|\mathbf{I}_n - \mathbf{A}|$ the determinant of $(\mathbf{I}_n - \mathbf{A})$.

As H tends to 0 the measurements do not improve the knowledge of the quantity to be retrieved. If $H > 0$ the entropy of the final state is less than the entropy of the initial state, therefore after the measurements the system results less chaotic, i.e. the measurements have improved the knowledge of the system.

3 Tropospheric Emission Spectrometer

The Tropospheric Emission Spectrometer (TES) (Beer et al., 2001) is one of the four instruments on board NASA's Aura satellite, launched on July 15, 2004. AURA is a sun-synchronous orbit satellite,

flying at an altitude of 705 km. Every 16 days, Aura re-examines the same portions of the atmosphere, and its instruments are able to measure changes that have occurred in each sampled area.

TES is a high-resolution, infrared, imaging Fourier-transform spectrometer with spectral coverage of 650-2250 cm^{-1} at a spectral resolution of 0.1-0.025 cm^{-1}, offering line-width-limited discrimination of essentially all radiatively active molecular species in the Earth's lower atmosphere. TES observes both straight down (nadir view) and at a sideways angle (limb view) behind the satellite. In this work only the TES nadir measurements have been considered.

Figure (1) shows the optical-filter specifications and the species in the atmosphere having absorption or emission features in the specified filter spectral ranges. Not all the filters are used in the global surveys. Filters 2B1, 1B2, 1A1, and 2A1 are used in nadir Global Surveys [2], and filters 2B1, 1B2, 1A1, 2A1, 1B1, and 2A4 are used in limb Global Surveys.

Filter Identification	Filter Half-Power Points (cm^{-1})		Major Species
Array 2B (650 - 900 cm^{-1})			
2B1	650	900	CO_2, HNO_3, CFC_{11}, NO_2
Array 1B (820 - 1150 cm^{-1})			
1B1	820	1050	HNO_3, NH_3, CFC_{11}, CFC_{12}, O_3
1B2	950	1150	O_3, NH_3, CFC_{11}, CFC_{12}, N_2O
Array 2A (1100 - 1950 cm^{-1})			
2A1	1100	1325	O_3, N_2O, HNO_3, CFC_{12}, SO_2, CH_4
2A2	1300	1550	O_3, HNO_3, CH_4
2A3	1500	1750	H_2O, NO_2
2A4	1700	1950	H_2O, NO
Array 1A (1900 - 3050 cm^{-1})			
1A1	1900	2250	O_3, CO, N_2O, NO, OCS
1A2	2200	2450	CO_2, N_2
1A3	2425	2450	N_2O
1A4	2600	2850	HDO
1A5	2800	3050	CH_4, HCl, O_3

Figure 1: TES optical-filter specifications and species absorbing or emitting in the filter spectral ranges.

Figure (2) shows the SO_2 optical thickness from 0 to 2500 cm^{-1}. The SO_2 optical thickness between 1000 and 1400 cm^{-1} is completely covered by 2A1 and 2A2 TES filters, but only the 2A1

[2]TES has two basic science operating modes: Global Surveys and Special Observations. Global surveys are the routine observations that TES conducts approximately every two days, which produce "standard products". Except for emergencies, Global Surveys are never interrupted. Special (Research) Observations include all other measurements, including those of validation and such events as volcano eruptions and biomass burning.

filter is used for nadir global surveys so only the 2A1 filter has been considered. In this spectral range the spectral resolution is 0.06 cm^{-1}.

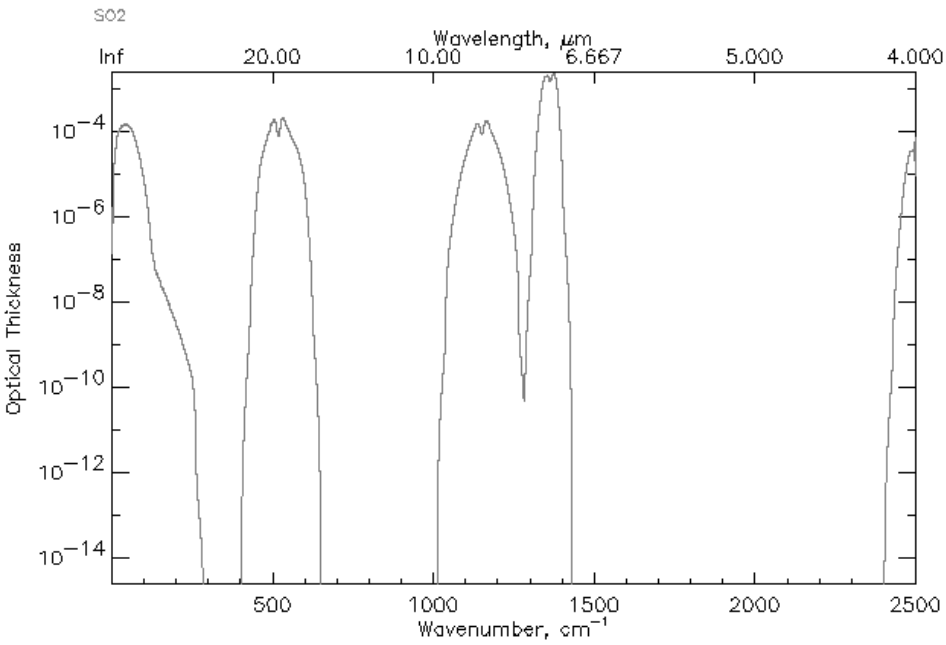

Figure 2: SO_2 optical thickness.

One of the features of a Fourier Transform Spectrometer (FTS) is that it readily supports an imaging mode, which, in turn, improves collection efficiency compared with the more traditional spatially scanning systems. TES employs 16 detectors, each of whose individual field of view is 0.75×7.5 mrad. In nadir mode this means a surface spatial resolution of 0.5 km in-track and 5 km cross-track (see Figure 3).

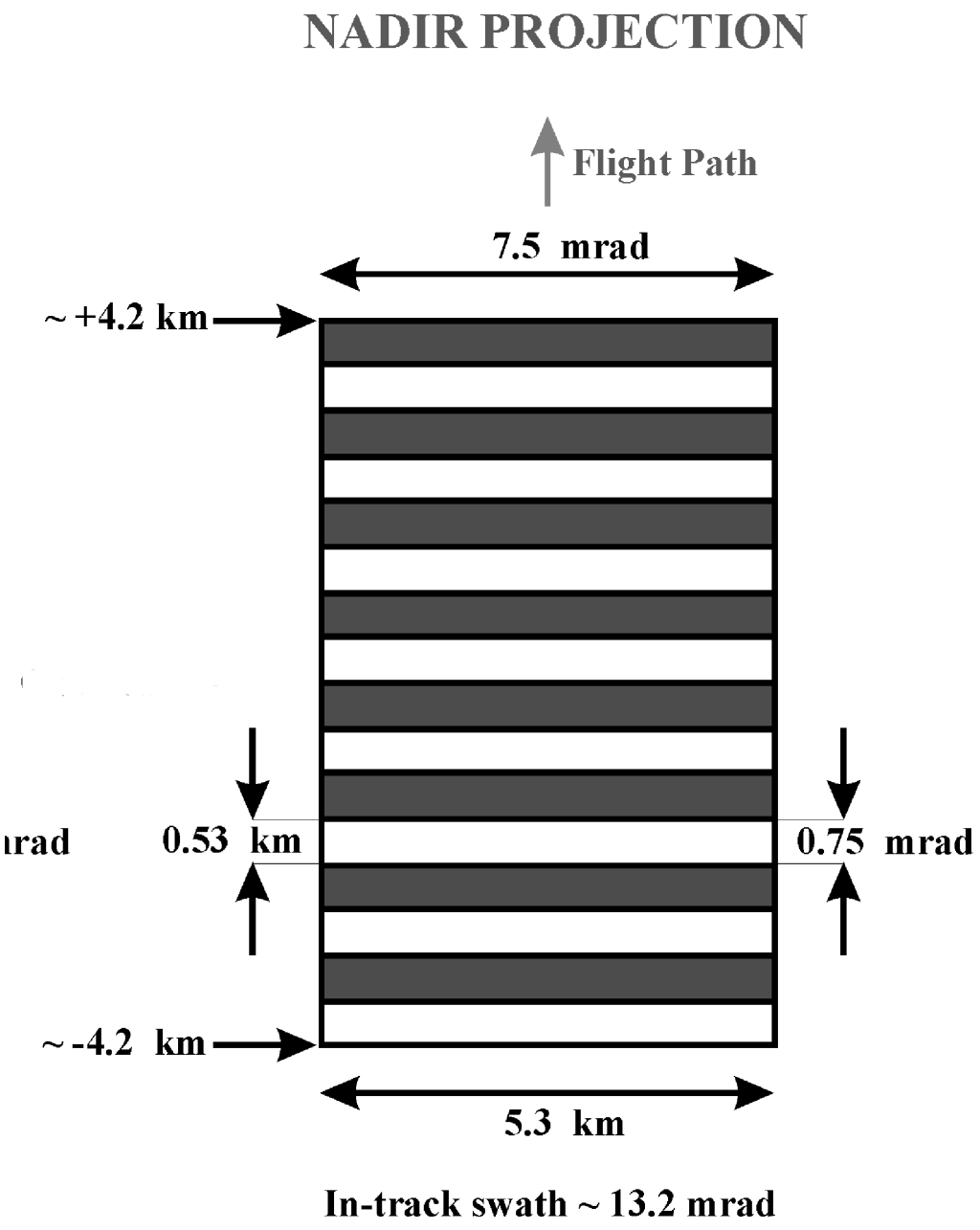

Figure 3: TES detector nadir projection.

4 Information content analysis

4.1 Characteristics of simulations

The information content for the SO_2 volcanic plume retrieval has been computed for TES nadir simulated data in the 2A1 spectral range considering two different SO_2 volcanic profile configurations: a *tropospheric configuration* and a *stratospheric configuration* (see Figure (4)). In the *tropospheric configuration*, approximating a quiescent volcanic emission, the plume is placed between 1 and 5 km, while in the *stratospheric configuration*, approximating a large volcanic eruption, the plume is placed between 9 and 13 km. The columnar amounts considered for each configuration are 10, 50, 100 and 150 DU (1 DU = 0.0285 g/,m^{-2}). All the simulations for the top of atmosphere (TOA) radiance and the SO_2 *weighting functions* have been carried out using the Radiative Forward Model (RFM) developed at the University of Oxford (http://www-atm.physics.ox.ac.uk/RFM/). The SO_2 WF have been computed for each wavenumber and for each element of the *state vector* composed of the SO_2 profile from 1 to 39 km with 2 km steps in altitude.

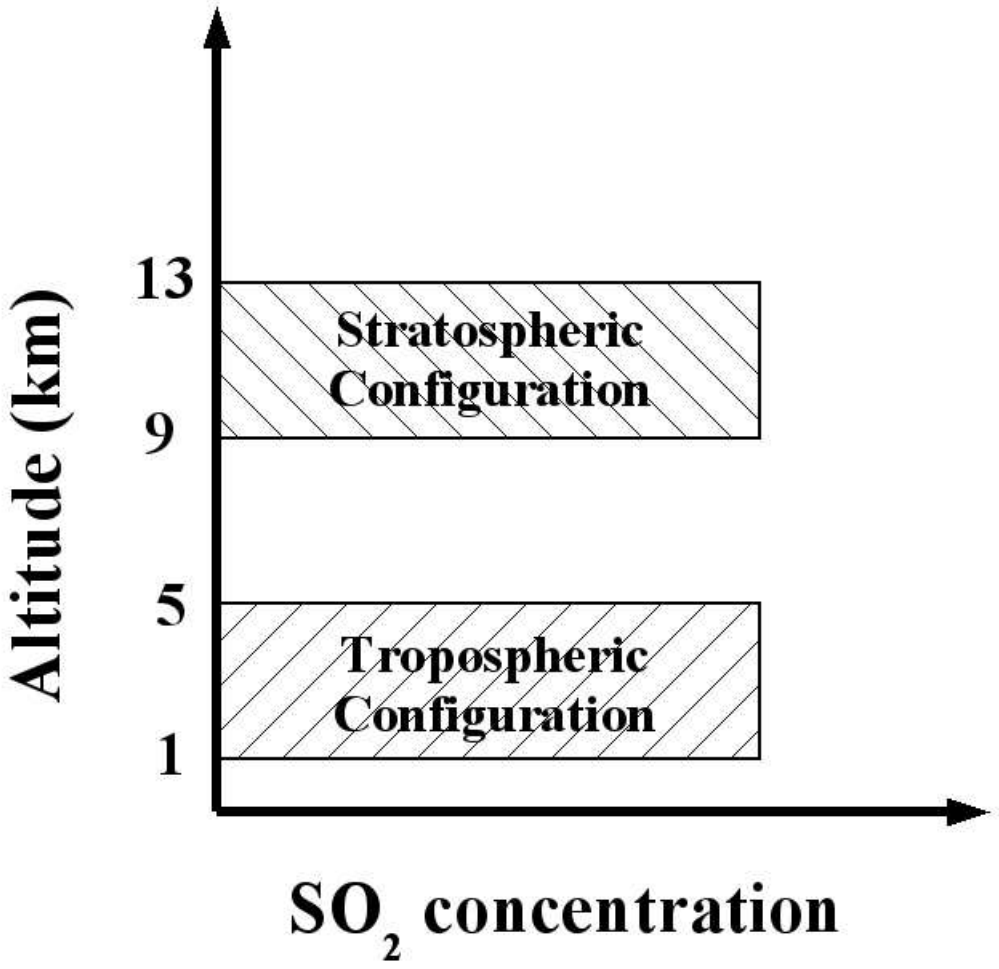

Figure 4: SO_2 plume configurations.

Figure (5) shows the radiance percentage difference between the TOA radiance computed con-

sidering the SO_2 default profiles and the TOA radiance computed considering a 50 DU SO_2 column amount in either configuration. It can be seen that even if we consider the same SO_2 amount in the troposphere or stratosphere, the TOA radiance variation is greater in the latter case. Figures (6) and (7) show the TOA radiance, the SO_2 profile and the SO_2 WF for a column amount of 50 DU in the *tropospheric* and *stratospheric* configuration respectively. As Figures (6) and (7) show the WF are

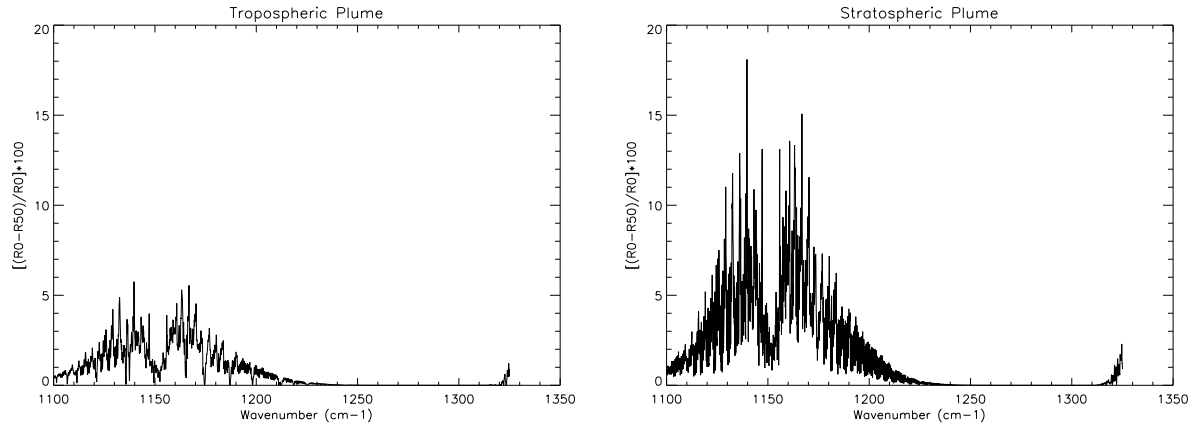

Figure 5: TOA radiance percentage difference between the default SO_2 profile and profile containing 50 DU; *tropospheric* (left) and *stratospheric* (right).

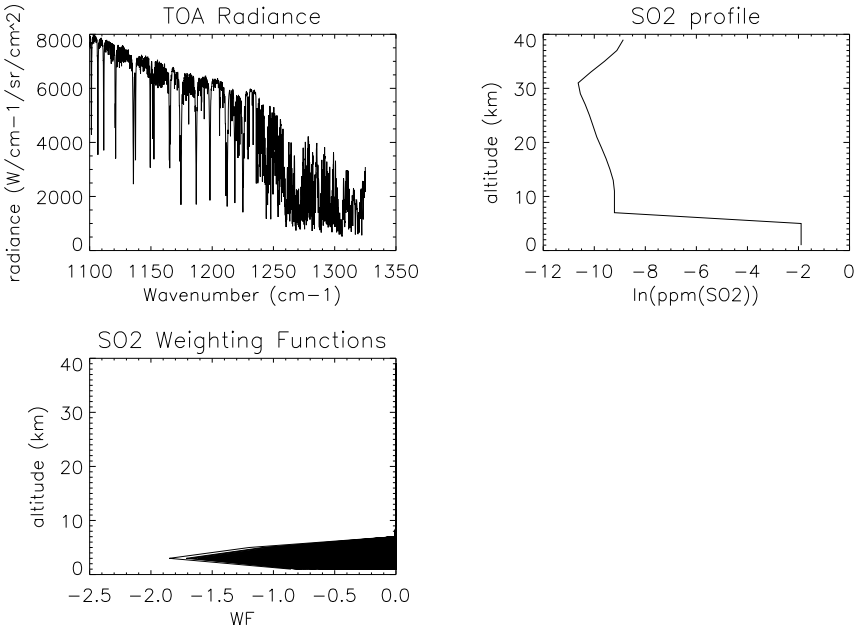

Figure 6: RFM simulation of 50 DU in the *tropospheric* SO_2 configuration. Top left: TOA radiance. Top right: SO_2 profile. Bottom left: SO_2 weighting functions

peaked at the levels where the SO_2 bulk is placed.

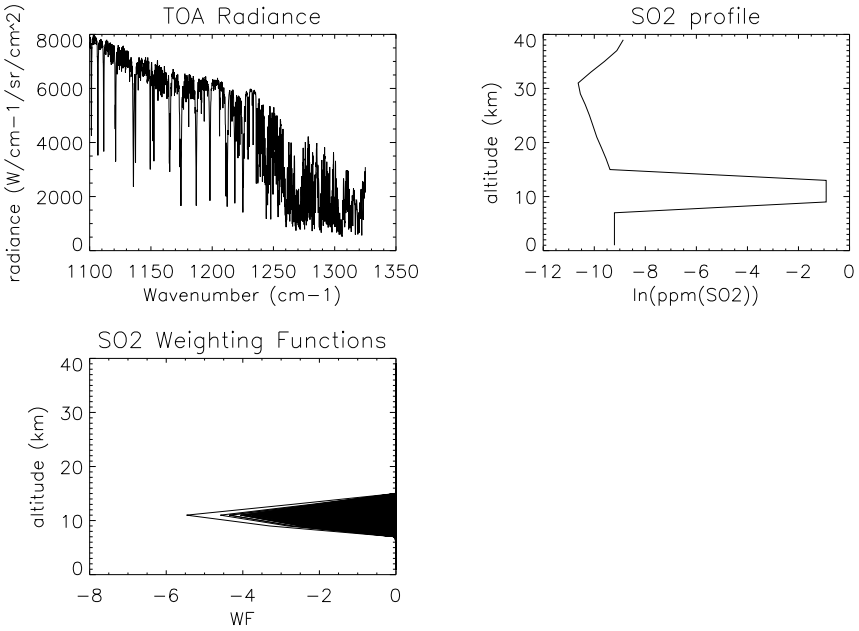

Figure 7: RFM simulation of 50 DU in the *stratospheric* SO_2 configuration. Top left: TOA radiance. Top right: SO_2 profile. Bottom left: SO_2 weighting functions

4.2 Information content setting parameters and results

To compute the information content the *measurement error* and the *a priori covariance* matrixes must be defined.

The *measurements covariance* matrix is diagonal i.e. no correlations between channels and between spectra from different detectors have been considered. The diagonal elements are the square root of the 16 detectors mean spectral noise for a given measurement. Figure (8) shows the mean spectrum and the mean noise over the 16 detectors and also the corresponding signal to noise ratio.

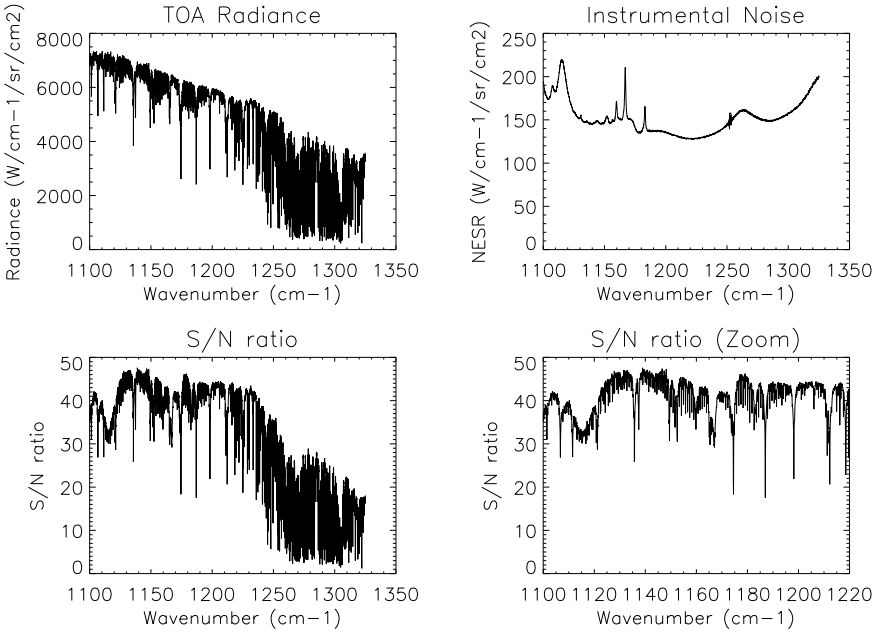

Figure 8: Mean spectrum and mean noise over the 16 detectors. Top left: mean TOA radiance. Top right: mean instrumental noise. Bottom left: signal-to-noise ratio. Bottom right: spectral zoom of the signal-to-noise ratio.

For the *a priori correlation* matrix an altitude correlation is considered (Rodgers, 1990; Rodgers, 2000):

$$\mathbf{S}_{a_{i,j}} = (\sigma_{a_{i,i}})^2 exp\left\{ - \mid i - j \mid \frac{\delta z_{i,j}}{h} \right\}, \forall (i \neq j) \tag{13}$$

where $\mathbf{S}_{a_{i,j}}$ are the *a priori correlation* matrix elements, $\sigma_{a_{i,i}}$ the a priori uncertainties, $\delta z_{i,j}$ is the level distance between the i and j layer mid-points and h is the *scale height*.

The a priori uncertainties have been set to 100 % for each level and the height correlation between levels to 3 km. Table (1) shows the DFS and H for the two different configurations considered. The information content is very low i.e. the measurements are not able to improve the knowledge of the a priori SO_2 profile in both *tropospheric* and *stratospheric* configurations. The measurements noise is too high for SO_2 retrieval in both *tropospheric* and *stratospheric* configurations. To reduce the instrumental noise the SVD approach has been considered.

Column Amount (DU)	DFS Troposphere	H Troposphere	DFS Stratosphere	H Stratosphere
10	0.00	0.00	0.00	0.00
50	0.00	0.00	0.06	0.04
100	0.02	0.02	0.45	0.43
150	0.10	0.08	0.77	1.07

Table 1: DFS and H for the different plume configurations.

5 Singular Vector Decomposition

Data vectors with several thousand elements (as for example the TES measurements) contain few degrees of freedom for signal and many degrees of freedom for noise: SVD is able to represent the signal in term of few coefficients that contain most of the information. The new data vector, called the *principal component* vector or *reconstructed* vector, consist of the components of the original vector in an orthogonal coordinate system and its elements are independent of each other (unlike the original vector). The SVD for high spectral resolution sounders (Huang et al., 2001; Goldberg et al., 2003) is used to reduce the measurements noise, giving the possibility to extract small signals from the spectra and improving the efficiency of the retrieval. In the first part of this section the SVD theory will be briefly presented and in the second part it will be applied to the TES nadir measurements.

5.1 Main Concepts

Singular vector decomposition (SVD) (Rodgers, 2000) is a method to solve the eigenvalue problem for a non-square matrix. Let $\mathbf{Y}$ be a non square matrix with *m* rows and *n* columns, the eigenvalue problem can be reconstructed by the symmetric problem:

$$\begin{bmatrix} 0 & \mathbf{Y} \\ \mathbf{Y}^T & 0 \end{bmatrix} \begin{bmatrix} \mathbf{u} \\ \mathbf{v} \end{bmatrix} = \gamma \begin{bmatrix} \mathbf{u} \\ \mathbf{v} \end{bmatrix} \tag{14}$$

where $\mathbf{v}$ and $\mathbf{u}$ are arrays of dimension *n* and *m* respectively. The vectors $\mathbf{v}$ and $\mathbf{u}$ are called *singular vectors* of $\mathbf{Y}$ and γ is the *singular value*. The symmetric eigenvalue problem is equivalent to the "shifted" eigenvalue problem:

$$\begin{aligned} \mathbf{Y}\mathbf{v} &= \gamma\mathbf{u} \\ \mathbf{Y}^T\mathbf{u} &= \gamma\mathbf{v} \end{aligned} \tag{15}$$

From equation (15) we can obtain by substitution:

$$\begin{aligned} \mathbf{Y}^T\mathbf{Y}\mathbf{v} &= \gamma\mathbf{Y}^T\mathbf{u} = \gamma^2\mathbf{v} \\ \mathbf{Y}\mathbf{Y}^T\mathbf{u} &= \gamma\mathbf{Y}\mathbf{v} = \gamma^2\mathbf{u} \end{aligned} \tag{16}$$

where $\mathbf{u}$ and $\mathbf{v}$ are the eigenvectors of $\mathbf{Y}\mathbf{Y}^T$ ($m\times m$) and $\mathbf{Y}^T\mathbf{Y}$ ($n\times n$) respectively, which have the same set of real eigenvalues. If the rank of $\mathbf{Y}$ is *p* then there will be *p* non zero singular values, and

both $\mathbf{Y}\mathbf{Y}^T$ and $\mathbf{Y}^T\mathbf{Y}$ will have *p* non-zero eigenvalues. Thus the eigenvectors with zero eigenvalues can be discarded and we can write:

$$\begin{bmatrix} 0 & \mathbf{Y} \\ \mathbf{Y}^T & 0 \end{bmatrix} \begin{bmatrix} \mathbf{U} \\ \mathbf{V} \end{bmatrix} = \mathbf{\Gamma} \begin{bmatrix} \mathbf{U} \\ \mathbf{V} \end{bmatrix} \tag{17}$$

where $\mathbf{\Gamma}$ is $p\times$ *p* diagonal matrix, $\mathbf{U}$ is $m\times$ *p* and $\mathbf{V}$ is $n\times$ *p*. There will be *n*+*m*-*p* more eigenvectors of the composite matrix, all with zero eigenvalues. The *singular values* and *vectors* have the following property:

$$\mathbf{Y} = \mathbf{U}\mathbf{\Gamma}\mathbf{V}^T = \sum_i \mathbf{u}_i \gamma_i \mathbf{v}_i^T \tag{18}$$

Because $\mathbf{U}^T\mathbf{Y}\mathbf{V} = \mathbf{\Gamma}$ we describe $\mathbf{U}$ as *left singular vectors* and $\mathbf{V}$ as *right singular vectors*. The *right vectors* $\mathbf{V}$ form an orthonormal basis in the row space and the *left vectors* form an orthonormal basis in the column space. The matrix $\mathbf{Y}$ maps the row space basis vector $\mathbf{v}$ into a corresponding column space basis vector $\mathbf{u}$, and $\mathbf{Y}^T$ maps $\mathbf{u}$ into $\mathbf{v}$. Thus $\mathbf{U}$ and $\mathbf{V}$ are a natural pair of coordinate systems for the two spaces.

5.2 Application to TES measurements

As a test case the SVD has been applied for 100 TES observations (i.e. 1600 spectra); the selected data contain the measurements made over the area where the Anatahan volcano eruption occurred on 5 April 2005. The Anatahan volcano is located in Mariana Islands in the Central Pacific Ocean (16.35° N, 145.67° E).

In this case the matrix $\mathbf{Y}$ is an ensemble of TES measured spectra i.e. the columns of $\mathbf{Y}$ are the TES spectra ($\mathbf{y}_j$). Following equation (18) the j^{th} individual spectrum ($\mathbf{y}_j$) can be obtained as:

$$\mathbf{y}_j = \sum_{i=1}^{n} \mathbf{u}_i \gamma_i v_{ij}^T \tag{19}$$

The spectrum is represented as a sum of columns $\mathbf{u}_i$ of $\mathbf{U}$, with coefficients $\gamma_i v_{ij}^T$.

The total number m of *singular vectors* is equal to the total number of channels, however a much smaller set of k *singular vectors*, ordered from largest to smallest associated *singular values*, is sufficient to explain most of the variability of the original spectra. Figure (9) shows the *singular values* of the selected ensemble of measurements.

Our choice of the number of *singular values* to consider is based on the consideration that nearly the 100 % of the spectra variability is explained with only twenty *singular values*. This number is often referred to as the number of independent pieces of information. These twenty *singular values* and the associated *singular vectors*, have been considered sufficient to reconstruct the radiance:

$$\tilde{\mathbf{y}}_j = \sum_{i=1}^{k} \mathbf{u}_i \gamma_i v_{ij}^T, (k = 20) \tag{20}$$

Because $\tilde{\mathbf{U}}^T\tilde{\mathbf{U}} = \mathbf{I}_k$ (of dimension $[m \times k]$) [3] the coefficients of equation (20) can be computed as:

$$\mathbf{c}_j = \tilde{\mathbf{U}}^T \mathbf{y}_j \tag{21}$$

[3]Note that $\tilde{\mathbf{U}}^T\tilde{\mathbf{U}} = \mathbf{I}_k$ but $\tilde{\mathbf{U}}\tilde{\mathbf{U}}^T \neq \mathbf{I}_m$

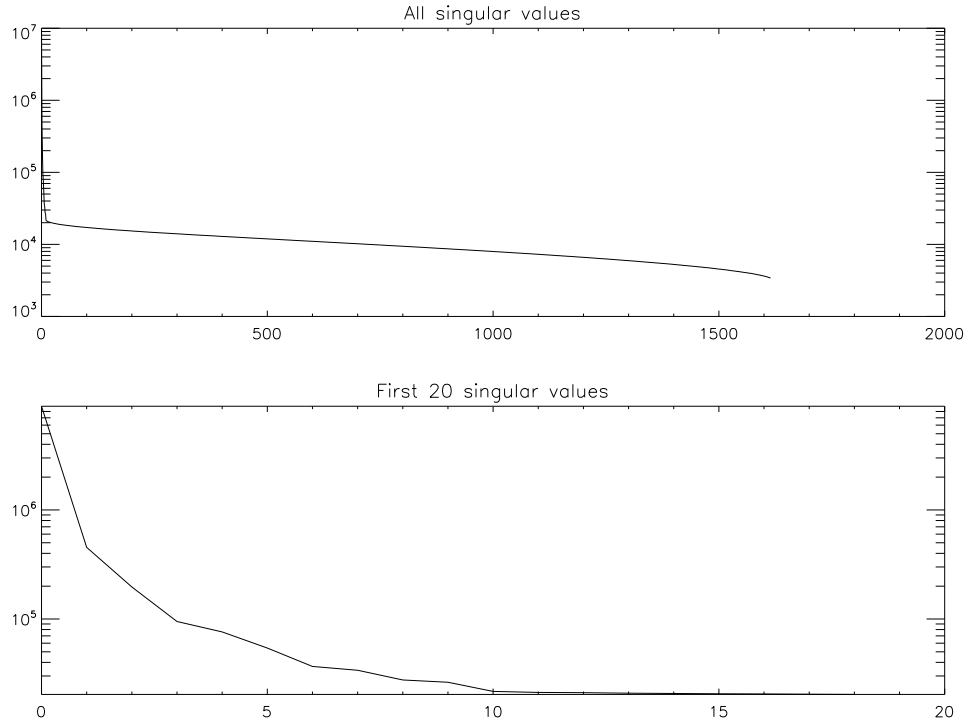

Figure 9: . Top: all singular values of the spectra ensemble selected. Bottom: first twenty singular values of the spectra ensemble selected.

with associated *coefficient error* (ϵ_{c_j}) and *covariance coefficient* matrix ($\mathbf{S}_{c_j}$) given by:

$$\epsilon_{c_j} = \tilde{\mathbf{U}}^T \epsilon_j \tag{22}$$

$$\mathbf{S}_{c_j} = \tilde{\mathbf{U}}^T \mathbf{S}_{\epsilon_j} \tilde{\mathbf{U}} \tag{23}$$

where ϵ_j is the j^{th} spectrum *measurement noise*.

Considering equation (21), equation (20) can be written as:

$$\tilde{\mathbf{y}}_j = \tilde{\mathbf{U}} \mathbf{c}_j = \tilde{\mathbf{U}} \tilde{\mathbf{U}}^T \mathbf{y}_j \tag{24}$$

The *reconstructed error* ($\tilde{\epsilon}_j$) and *reconstructed covariance* ($\tilde{\mathbf{S}}_\epsilon$) are:

$$\tilde{\epsilon}_j = \tilde{\mathbf{U}} \tilde{\mathbf{U}}^T \epsilon_j \tag{25}$$

$$\tilde{\mathbf{S}}_\mathbf{j} = \tilde{\mathbf{U}} \tilde{\mathbf{U}}^T \mathbf{S}_{\epsilon_j} \tilde{\mathbf{U}} \tilde{\mathbf{U}}^T \tag{26}$$

Inserting the (23) into (26) we obtain:

$$\tilde{\mathbf{S}}_j = \tilde{\mathbf{U}} \mathbf{S}_{c_j} \tilde{\mathbf{U}}^T \tag{27}$$

The resulting *reconstructed covariance* matrix, $\tilde{\mathbf{S}}_\mathbf{j}$, is singular.

Figure (10) and (11) show the original and the reconstructed spectrum and the original and the reconstructed noise respectively for a selected spectrum contained in the ensemble using the first 20

singular values. The reconstructed noise has been computed as the square root of the *reconstructed noise correlation* matrix ($\tilde{\mathbf{S}}_j$) diagonal elements. As Figure (11) show after the SVD application the measurements reconstructed noise results two order of magnitude lower than the original noise.

The information content has been computed considering the *reconstructed covariance matrix* and

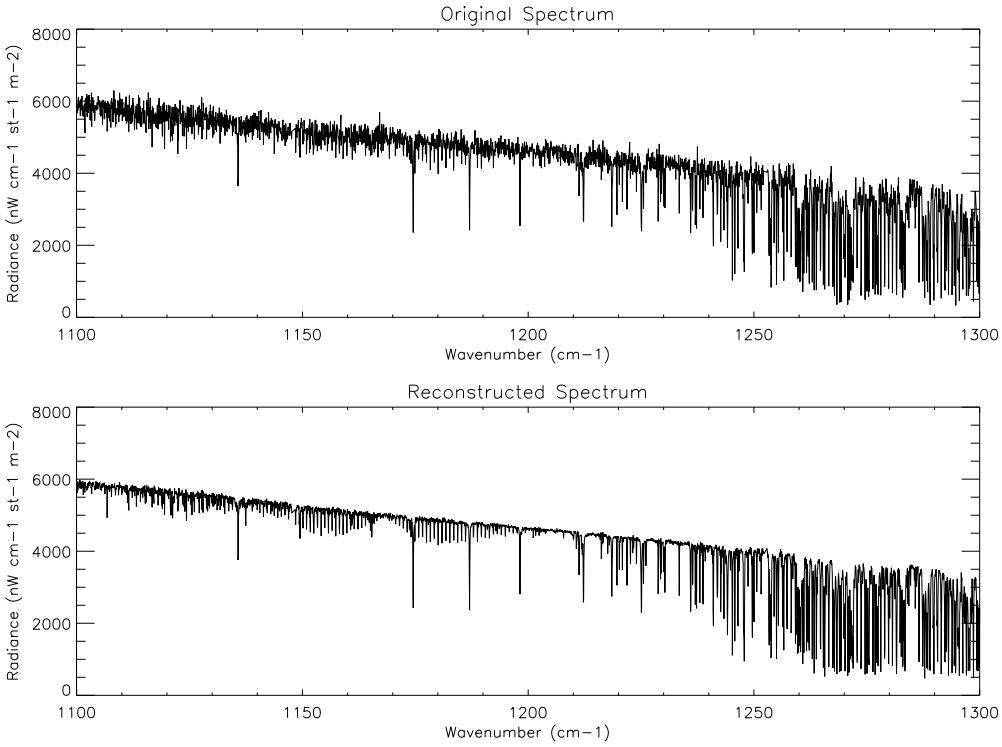

Figure 10: Top: original spectrum. Bottom: reconstructed spectrum using the first 20 singular values.

the same a priori matrix defined before (see Section (4.1)). Table (2) shows the DFS and H for the two different configurations considered. Figure (12) and (13) show the *averaging kernel* and the *total*

Column Amount (DU)	DFS Troposphere	H Troposphere	DFS Stratosphere	H Stratosphere
10	2.41	7.76	1.95	12.57
50	3.42	17.76	3.05	20.37
100	3.01	22.42	3.00	21.45
150	3.00	24.92	3.00	21.57

Table 2: DFS and H for the different plume configurations considering the reconstructed noise covariance matrix ($\tilde{S}$).

retrieval error for 50 DU of SO_2 columnar content for *tropospheric* and *stratospheric* configurations respectively.

Using the SVD approach the information content (see Table (2)) increases meaningfully. Looking at the *averaging kernel* of Figures (12) and (13) it can be seen that each *averaging kernel* curve peak

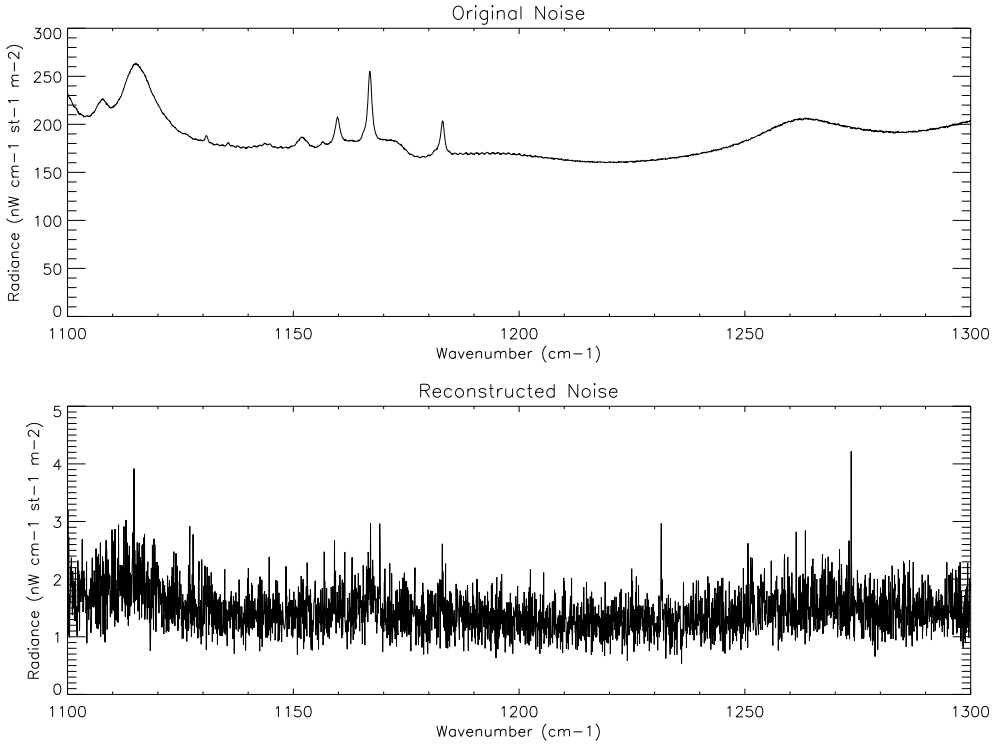

Figure 11: Top: original spectrum noise. Bottom: reconstructed spectrum noise using the first 20 singular values.

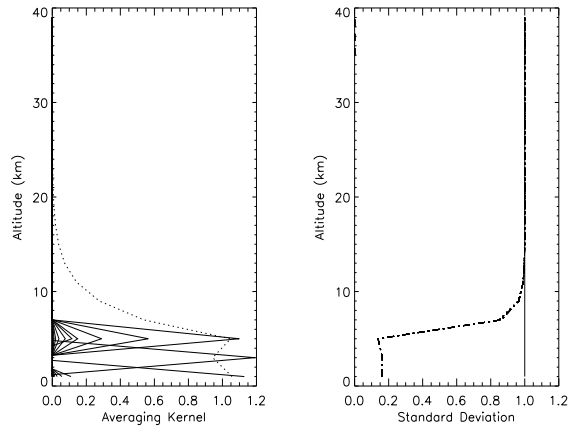

Figure 12: 50 DU SO_2 columnar content - *tropospheric* configuration. Left: the solid lines represents the *averaging kernel* while the dotted line is the sum of *averaging kernel* rows. Right: the solid line is the a priori standard deviation and the dash-dot line is the *total retrieval error*.

is located at the right level, where the SO_2 is placed. The area of $\mathbf{A}$ is approximately unity from 1 to 5 km and from 9 to 13 km, indicating that the retrieval is sensitive to the true profile over these height ranges. The same consideration can be done looking at the *retrieval error* plot of the same figures where an improvement of a-priori standard deviation occurred at the altitude where SO_2 is.

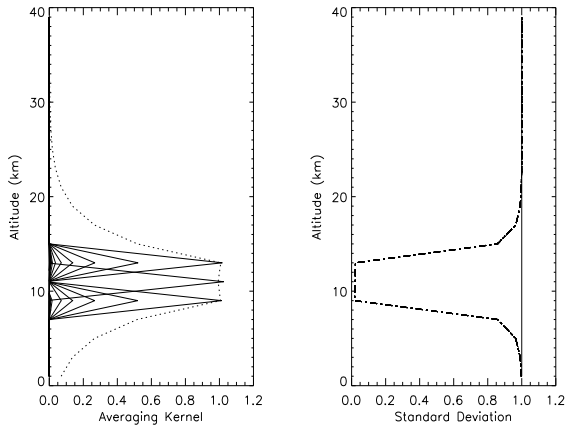

Figure 13: 50 DU SO_2 columnar content - *stratospheric* configuration. Left: the solid lines represents the *averaging kernel* while the dotted line is the sum of *averaging kernel* rows. Right: the solid line is the a priori standard deviation and the dash-dot line is the *total retrieval error*.

6 Microwindow selection

High spectral resolution instruments provide more channels than can be used, or are needed because of duplication of information. We must define a criteria to select channels or microwindows that contain most of the measurement information.

For the optimisation of a measurement method a single scalar figure of merit is required. There are two quantities of general applicability which can be defined without reference to the specific retrieval method; these are the degrees of freedom for signal and the variation of entropy. The basic strategy is to consider microwindows, of selected width, independently and sequentially (Rodgers 1998; Dudhia et al., 2002). Starting with no microwindow selected: (1) compute the information content of each microwindow of the entire spectral range; (2) select the microwindow providing the most information; (3) repeat until enough information has been gathered.

The microwindows width has been set equal to $3\,\mathrm{cm}^{-1}$ and the procedure has been applied considering the two different plume configurations (*tropospheric* and *stratospheric*) and the different column amounts of SO_2 (10, 50, 100 and 150 DU). For each microwindow the information content has been computed considering 100 % of a priori profile uncertainty (with 3 km *scale height*) and as *measurement covariance* matrix the *reconstructed covariance* matrix computed using the SVD approach described in the previous Section.

Figure (14) and (15) show the microwindows selected, by the procedure described, for the two configurations. The figures show that almost all the microwindows selected, with high information

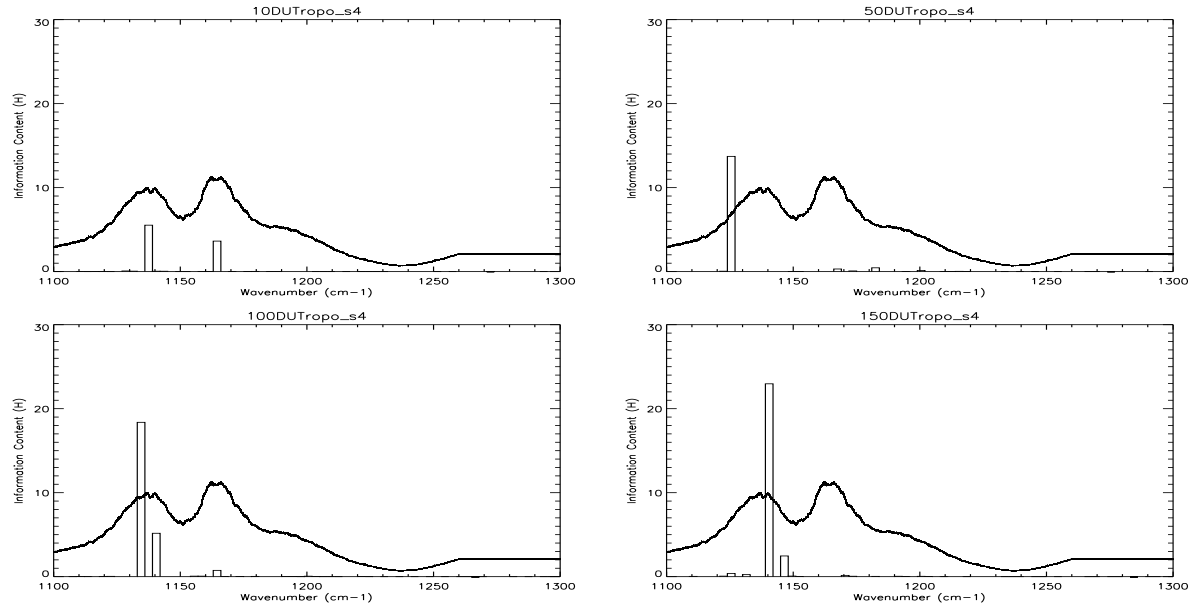

Figure 14: Micro-windows for Tropospheric plume configuration. Top left: SO_2 columnar content=10 DU. Top right: SO_2 columnar content=50 DU. Bottom right: SO_2 columnar content=100 DU. Bottom left: SO_2 columnar content=150 DU. The solid line is the smoothed SO_2 cross section (multiplying by a 10^{22} factor)

content, are within the SO_2 cross-section peak spectral range i.e. as expected the microwindows selected coincide with the maximum of the SO_2 absorption.

Table 3 summarises the spectral ranges of the microwindows selected with an information content greater than 1 (as shown in Figures (14) and (15)). As Table 3 shows the microwindows selected

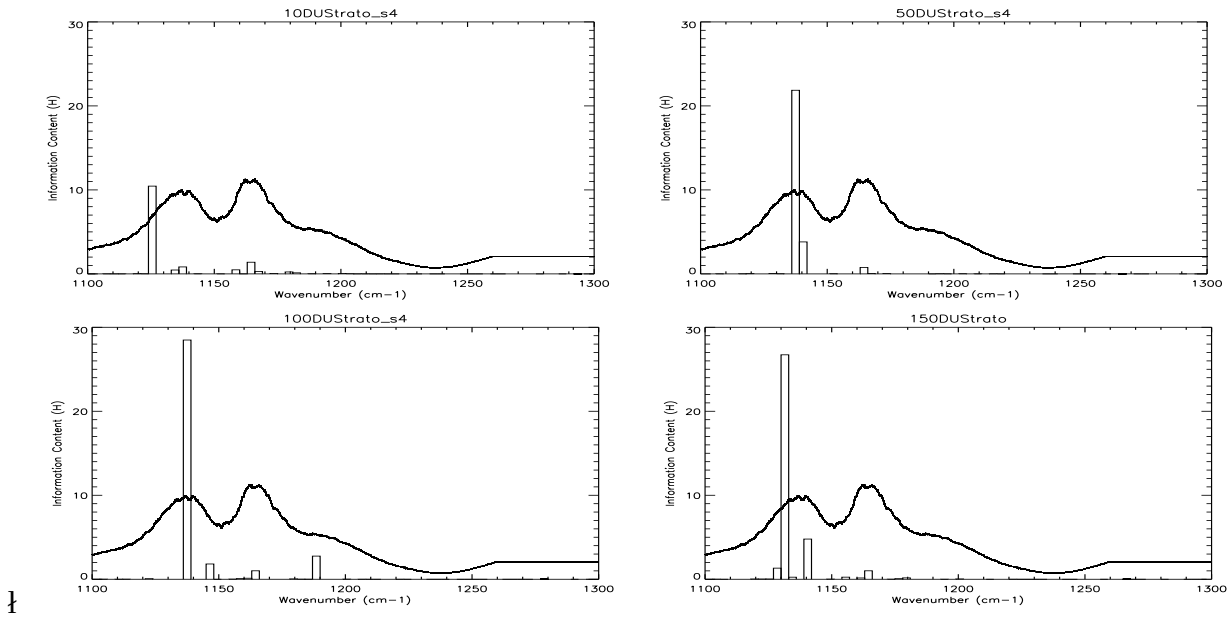

Figure 15: Micro-window for Stratospheric plume configuration. Top left: SO_2 columnar content=10 DU. Top right: SO_2 columnar content=50 DU. Bottom right: SO_2 columnar content=100 DU. Bottom left: SO_2 columnar content=150 DU. The solid line is the smoothed SO_2 cross section (multiplying by a 10^{22} factor).

Columnar Content (DU)	MCW *Tropospheric*	MCW *Stratospheric*
10	[1136.02-1139.02]	[1124.02-1127.02]
	[1163.02-1166.02]	[1163.02-1166.02]
50	[1124.02-1127.02]	[1136.02-1139.02]
		[1139.02-1142.02]
100	[1133.02-1136.02]	[1136.02-1139.02]
	[1139.02-1142.02]	[1145.02-1148.02]
		[1187.02-1190.02]
150	[1145.02-1148.02]	[1130.02-1133.02]
		[1127.02-1130.02]

Table 3: SO_2 retrieval microwindows for *tropospheric* and *stratospheric configurations*.

for the two *tropospheric* and *stratospheric configurations* are approximately the same: except the 1133.02-1136.02 cm^{-1} microwindow, all the other microwindows selected for the *tropospheric configuration* has been found also for the *stratospheric configuration*.

For the SO_2 volcanic profile retrievals all the microwindows selected will be considered. These microwindows are given in Table (4).

MCW	Spectral Range
1	[1124.02-1127.02]
2	[1127.02-1130.02]
3	[1130.02-1133.02]
4	[1133.02-1136.02]
5	[1136.02-1139.02]
6	[1139.02-1142.02]
7	[1145.02-1148.02]
8	[1163.02-1166.02]
9	[1187.02-1190.02]

Table 4: Microwindows selected for SO_2 profile retrieval.

7 Conclusions

In this work has been investigated the feasibility of the use of the TES nadir measurements for the SO_2 volcanic plume columnar abundance and altitude retrieval.

The analysis has been carried out considering two different plume configurations, *tropospheric* (plume bulk between 1 and 5 km) and *stratospheric* (plume bulk between 9 and 13 km), considering an SO_2 columnar abundance of 10, 50, 100 and 150 DU. The SO_2 *weighting functions*, needed for the information content analysis, have been computed using the Radiative Forward Model developed at the Atmospheric Oceanic and Planetary Physics Department (AOPP) of the Oxford University, for each element of the *state vector* composed of an SO_2 profile from 1 to 39 km in steps of 2 km.

The information content analysis shows that the instrumental noise is too high for this kind of retrieval, i.e. the measurements are not able to improve the knowledge of the system. In all the cases considered, the degrees of freedom for signal results are less than 1.

To reduce the TES instrumental noise the singular vector decomposition (SVD) approach has been applied. The SVD has been applied to 100 TES nadir observations (1600 spectra) over an area containing the Anatahan volcano (Mariana Islands, Central Pacific Ocean) on 5 April 2005, when a volcanic eruption occurred. The first 20 singular values has been used to reconstruct the TES spectrum and noise. The *reconstructed measurements covariance* matrix is singular and the square root of its diagonal elements, i.e. the *reconstructed measurement errors*, are two orders of magnitude lower than the original noise. The information content increases meaningfully reaching 3 DFS, the maximum obtainable from the configurations selected.

A procedure, based on the optimisations of a single figure of merit, has been applied for the 3 cm^{-1} microwindows selection, considering the SVD reconstructed data. As expected almost all the microwindows selected fall into the maximum SO_2 absorption spectral range and for the two configuration considered the microwindows results approximately the same. For the SO_2 columnar abundance and altitude retrieval purpose all the microwindows selected will be considered.

References

Beer, R., Glavich T. A., and Rider D. M., 2001, Tropospheric emission spectrometer for the Earth Observing System's Aura satellite, Applied Optics, 40, pp.2356-2367.

Caltabiano, T., Romano, R. and Budettta, G., 1994, SO2 Flux measurements at Mt. Etna. Journal of Geophysical Research, D6, pp.12809-12819.

Casadevall, T. J. et al., 1987, In Volcanism in Hawaii US Geol. Soc. Prof. Paper, 1350, pp.771-780 (US Geol. Soc., Washington DC).

Casadevall, T.J., 1994, Volcanic ash and aviation safety. US Geological Survey Bulletin, 2047, pp.1-6.

Dudhia, A., Jay, V.L., Rodgers, C.D., 2002, Microwindow selections for high spectral resolution sounders. Applied Optics, 41, 8, pp.3665-3673.

Gerlach, T. M., Graeber, E. J., 1985, Volatile budget of Kilauea volcano. Nature, 313, pp.273-277.

Goldberg, M.D., Qu, Y., McMillin, L.M., Wolf, W., Zhou, L., Divakarla, M., 2003, AIRS Near-Real-Time Products and Algorithms in Support of Operational Numerical Weather Prediction. IEEE Transaction on Geoscience and Remote Sensing, 41, pp.379-389.

Grainger, R. G., Lambert, A., Taylor, F. W., Remedios, J. J., Rodgers, C. D., Corney, C. D., Kerridge B. J., 1993. Infrared absorption by volcanic stratospheric aerosols observed by ISAMS. Geophysical Research Letter, 20, pp.1283-1286.

Grainger, R. G. and Highwood E. J., 2003. Changes in stratospheric composition chemistry, radiation and climate caused by volcanic eruptions. Volcanic Degassing, Geological Society, London, Special Publication, 213, edited by Oppenheimer C., Pyle D. M., and Barklay M., pp.329-347.

Huang H.L., Antonelli P., 2001, Application of Principal Component Analysis to High-Resolution Infrared Measurement Compression and Retrieval. Journal of Applied Meteorology, 40 pp.356-388.

Krueger, A.J., 1983, Sighting of El Chichon sulphur dioxide clouds with the Nimbus 7 total ozone mapping spectrometer. Science, 220, pp1377-1379.

Krueger, AJ, Walter, LS, Schnetzler, CC and Doiron, SD, 1990, TOMS measurement of the sulphur dioxide emitted during the 1985 Nevado del Ruiz eruptions. Journal of Volcanology and Geothermal Research, 41, pp.7-15.

Malinconico Jr., L.L., 1979, Fluctuations in SO2 emission during recent eruptions of Etna. Nature, 278, pp.43-45.

Malinconico Jr. L.L., 1987, On the variation of SO2 emission from volcanoes. Journal of Volcanology and Geothermal Research, 33, pp.231-237.

Prata, A. J., Rose, W. I., Self, S., and O'Brien D. M., 2003, Global, long-term sulphur dioxide measurements from TOVS data: A new tool for studying explosive volcanism and climate. Volcanism and Earth's Atmosphere, Geophysics Monograph, 139, pp.75-92.

Prata A. J. and Bernardo C. Retrieval of volcanic SO_2 total column from AIRS data. Submitted.

Read, W. G., Froidevaux L., and Waters, J. W., 1993, Microwave Limb Sounder (MLS) measurements of SO_2 from Mt. Pinatubo volcano. Geophysical Research Letter, 20, pp.1299-1302.

Rodgers, C.D., 1990, Characterization and error analysis of profiles retrieved from remote sounding experiments. Journal of Geophysical Research, 95, 5587.

Rodgers, C.D., 1998, Information content and optimization of high spectral resolution measurements. Advanced Space Research, 21, 3, pp.361-367.

Rodgers, C.D., 2000, Inverse methods for atmospheric sounding. World Scientific Publishing Pte Ltd, New York.

Stenchikov, G., Kirckner, I. et al., 1998. Radiative forcing from the 1991 Mount Pinatubo volcanic eruption. Journal of Geophysical Research, 103, pp. 13837-13857.

Urai, M., 2004, Sulphur dioxide flux estimation from volcanoes using Advanced Spaceborne Thermal Emission and Reflection Radiometer - a case study of Miyakejima volcano, Japan. Journal of Volcanology and Geothermal Research, 134, pp.1-13.

Watson, I.M., Realmuto, V.J., Rose, W.I., Prata, A.J., Bluth, G.J.S., Gu, Y., Bader, C.E. and Yu, T., 2004, Thermal infrared remote sensing of volcanic emissions using the moderate resolution imaging spectroradiometer. Journal of Volcanology and Geothermal Research, 135, pp.75-89.